
Simulation of Transport in Partially Miscible Binary Fluids: Combination of Semigrandcanonical Monte Carlo and Molecular Dynamics Methods

Kurt Binder, Subir K. Das, Jürgen Horbach, Marcus Müller, Richard Vink, and Peter Virnau

Institut für Physik, Johannes Gutenberg-Universität Mainz, Staudinger Weg 7, D-55099 Mainz, Germany, Kurt.Binder@uni-mainz.de

Binary Fluids that exhibit a miscibility gap are ubiquitous in nature (glass melts, polymer solutions and blends, mixtures of molten metals, etc.) and exhibit a delicate interplay between static and dynamic properties. This is exemplified for a simple model system, the symmetrical AB Lennard–Jones mixture. It is shown how semigrandcanonical Monte Carlo methods, that include $A \rightarrow B$ ($B \rightarrow A$) identity switches as Monte Carlo moves, can yield the phase diagram, the interfacial tension between coexisting phases, and various pair correlation functions and structure factors. In addition to the build-up of long-ranged concentration correlations near the critical point, unmixing is also accompanied by the build-up of subtle structural features on very small length scales (less than the Lennard–Jones diameters).

System configurations, that are well equilibrated by these Monte Carlo methods, can be favorably used as initial states for Molecular Dynamics runs in the microcanonical ensemble. In this way it is possible to study the behavior of transport coefficients as well as dynamic correlation functions precisely along the coexistence curve, as well as for other paths in the one-phase region of the phase diagram.

1 Introduction

It has been a longstanding problem of physics and chemistry (and of materials science) to clarify the relationship between dynamic properties of fluid or solid matter, and the phase transitions which these systems undergo, in particular, phase separation. Typical materials are multicomponent metallic alloys, oxide mixtures, polymer solutions, and polymer blends [Kos01]. Phase separation in a polymer mixture is a multiscale problem — the polymer coil exhibits nontrivial structure from the scale of the length of covalent bonds (1 Å) to

the scale of the gyration radius (100 Å), and in the critical region near the critical point of unmixing the correlation length of concentration fluctuations may be as large as 1000 Å [Bin94]. Also the dynamics extends over many decades in time, from 10^{-13} seconds to macroscopic times [Bin95].

Sometimes phase separation competes with crystallization, for instance in the mixture of molten silicon dioxide and aluminium oxide. Again this is a multiscale problem: in the fluid there is nontrivial structure from the scale of covalent bonds to the medium range order that characterizes the continuous random network of this glassformer already in the melt far away from any phase transition [BK99]. Near the unmixing critical point we have again a large correlation length of concentration fluctuations. Also in this example the dynamics extends from subpicoseconds to macroscopic times, due to the proximity of the glass transition [Jae86]. This list of examples could be easily continued.

Dealing with chemically realistic models of such systems is still a major unsolved challenge. In this review we hence describe the state of the art of what can be done today by presenting a simple model system, the symmetrical binary AB Lennard–Jones mixture, and we will explain the appropriate methods of study. Then a selection of both static properties (phase diagram, interfacial tension, various radial distribution functions and structure factors that convey information on the unmixing) and quantities characterizing the dynamics (coherent and incoherent intermediate dynamic structure factors, wavenumber dependent relaxation times, selfdiffusion and interdiffusion constants, viscosity) will be defined and discussed. Emphasis always will be on the methodological aspects of such simulations.

2 A simple model: the symmetrical Lennard–Jones mixture

Following [DHB03] we choose a fluid of point particles located in continuous space (in a box of finite volume $V = L^3$ with periodic boundary conditions) and interacting with the potential

$$u(r_{ij}) = 4\epsilon_{\alpha\beta} \left[(\sigma_{\alpha\beta}/r_{ij})^{12} - (\sigma_{\alpha\beta}/r_{ij})^6 \right], \quad r_{ij} = |\mathbf{r}_i - \mathbf{r}_j|, \quad \alpha, \beta \in \text{A, B}. \quad (1)$$

The Lennard–Jones parameters $\{\epsilon_{\alpha\beta}, \sigma_{\alpha\beta}\}$ are chosen as follows

$$\sigma_{AA} = \sigma_{AB} = \sigma_{BB} = \sigma, \quad \epsilon_{AA} = \epsilon_{BB} = \epsilon. \quad (2)$$

Eq. (2) defines precisely what is meant by “symmetric mixture”. In the following, units of length, temperature, and energy are chosen by requiring that $\sigma = 1$, $\epsilon = 1$, and Boltzmann’s constant $k_B = 1$. In the Molecular Dynamics (MD) part, also the masses are chosen as $m_A = m_B = m = 1$. In the Monte Carlo (MC) part, masses cancel out since we work with classical statistical mechanics (see e.g. [BC96] for a general introduction into MC and MD).

If the remaining energy parameter ϵ_{AB} would also be chosen as $\epsilon_{AB} = \epsilon$ ($= 1$) one would have the trivial problem of an ideal mixture. So $\delta = \epsilon_{AB}/\epsilon = 0.5 < 1$ is chosen: this leads to unmixing, because less energy is won for AB pairs rather than for AA and BB pairs (at the preferred distance $2^{1/6}\sigma$). As usual, the potential is truncated and shifted to zero at $r_{ij} = 2.5\sigma$ [BC96]. In order to stay away from the gas-liquid transition as well as from crystallization, a density $\rho = 1$ is chosen. This ensures that the system stays in the fluid phase for the temperature range of interest, $1 \leq T \leq 2$ (note that the critical temperature of unmixing is $T_c \approx 1.638$, see below).

3 General comments on simulation methods

A first equilibration run is done with MC in the $N_A N_B VT$ ensemble for $N_A = N_B$ with standard trial displacements of particle coordinates in the range $[-\sigma/20, +\sigma/20]$, running for 100000 Monte Carlo steps (MCS) per particle. Then the semigrandcanonical MC algorithm is switched on: at the end of each displacement step per particle an attempted switch of $N/10$ randomly chosen particles is made, $A \rightarrow B$ or $B \rightarrow A$ (N denotes the total number of particles). These moves are accepted or rejected according to the standard Metropolis algorithm [BC96], but now both the energy change ΔE and the change of the chemical potential difference $\pm \Delta\mu$ needs to be taken into account in the Boltzmann factor. The independently fixed variables of the semigrandcanonical ensemble are total particle number N , volume V , temperature T , and chemical potential difference $\Delta\mu$, while the relative concentrations $x_A = N_A/(N_A + N_B) = N_A/N$, $x_B = N_B/N (= 1 - x_A)$ are fluctuating variables. Their average values $\langle x_A \rangle$, $\langle x_B \rangle$ are an output rather than an input to the simulation! The symmetry between A and B in our model dictates that for the choice $\Delta\mu = 0$ we have $\langle x_B \rangle = 1/2$ for $T > T_c$, while for $T < T_c$ one obtains states at the coexistence curve. The location of the coexistence curve shows up via peaks in the distribution function of the relative concentration $P(x_A)$, see Fig. 1.

In principle, for finite systems there is no symmetry breaking possible in full thermal equilibrium [BH02]. So for $T < T_c$, one should always observe two peaks, one at $x_A^{\text{coex}(2)}$ and the other at $x_A^{\text{coex}(1)}$, corresponding to the two branches of the coexistence curve. In practice, the two branches are separated at low temperatures by a huge free energy barrier. Therefore, with 400000 MCS “ergodicity breaking” [BH02] occurred for $T = 1.2$ and $T = 1.4$, i.e. only the A rich phase but not the B rich phase was observed. For $T = 1.6$, however both phases could be observed.

One can avoid “ergodicity breaking” by applying biased sampling techniques such as “successive umbrella sampling” [VM03] which then also yields quantitative information on the mentioned free energy barrier. In fact, one then can extract information on the surface tension between coexisting A-rich and B-rich phases from such a calculation, applying the formula [Bin82]

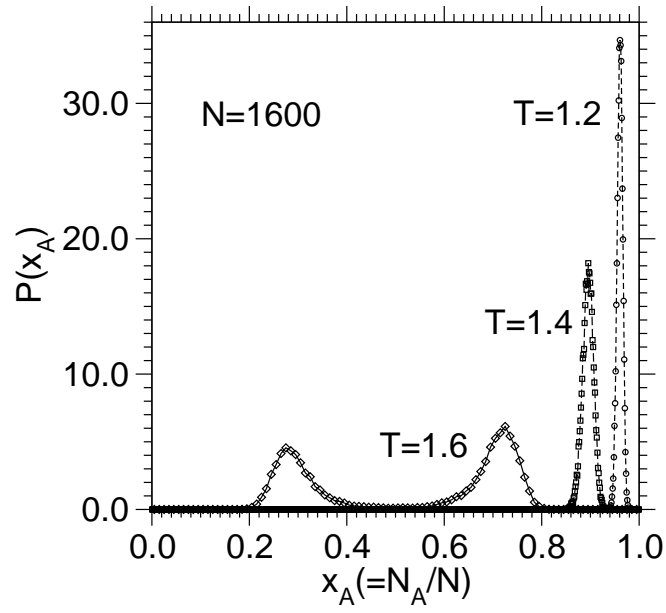


Fig. 1. Distribution function $P(x_A)$ for the relative concentration x_A of A particles for $N = 1600$ at $\Delta\mu = 0$ and the three temperatures indicated. From [DHB03].

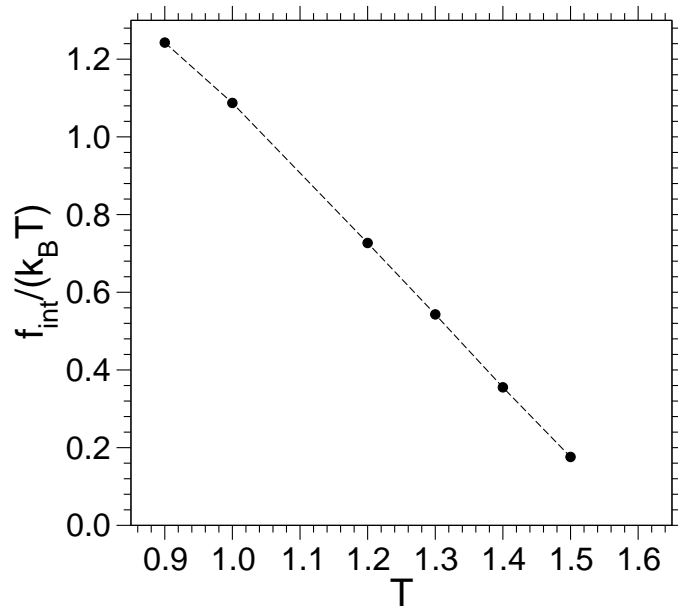


Fig. 2. Surface tension $f_{\text{int}}/(k_B T)$ of the symmetrical binary Lennard-Jones mixture plotted vs. temperature.

$$\frac{f_{\text{int}}}{k_B T} = \lim_{L \rightarrow \infty} \frac{1}{2L^2} \ln \{ P^{(\text{max})}(x_A) / P^{(\text{min})}(x_A) \} . \quad (3)$$

Fig. 2 shows the result of such a calculation for $N = 800$. The MC data are indeed compatible with the expected critical vanishing of f_{int} at T_c , $f_{\text{int}} \propto (T_c - T)^{2\nu}$ where $\nu \approx 0.63$ [Bin82].

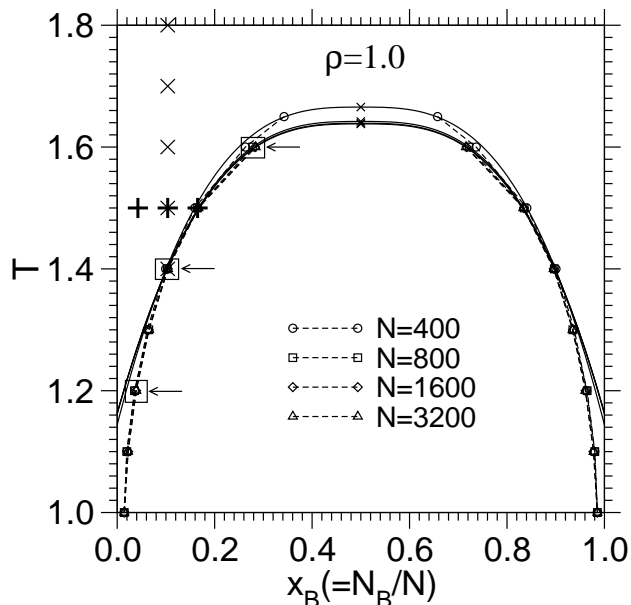


Fig. 3. Phase diagram of the symmetrical binary Lennard–Jones mixture, including results for four choices of N , as indicated. Crosses at $x_B = 0.10375$, plus symbols at $T = 1.5$ and squares with arrows indicate paths in the (T, x_B) plane for which the static and dynamical behavior was studied. From [DHB03].

Fig. 3 shows the phase diagram of the symmetrical binary Lennard–Jones mixture. While the broken curve is a guide to the eye for the coexistence curve separating the two–phase region (inside of the curve) from the one–phase region (outside of it), the full curves are phenomenological fits to the expected power law [BH02, BC96],

$$x_B^{\text{crit}} \pm x_B^{\text{coex}} = \hat{B}(1 - T/T_c)^\beta, \quad \beta \approx 0.325 \quad , \quad (4)$$

where \hat{B} is a so–called “critical amplitude” and of course, $x_B^{\text{crit}} = 1/2$, due to the symmetry of the model. From Fig. 3 it is clear that $N = 400$ is too small to allow reliable estimates, but for $N \geq 800$ the finite size effects are small, and the analysis of the MC data with Eq. (4) yields $T_c = 1.638 \pm 0.005$. If higher accuracy were desired, a finite size scaling analysis [BC96, BH02] needed to be performed.

Due to the symmetry between A and B, “ergodicity breaking” is no problem at all here for locating the coexistence curve: one may normalize $P(x_A)$ such that

$$\int_{1/2}^1 P(x_A) dx_A = 1, \quad x_A^{\text{coex}(2)} = \int_{1/2}^1 x_A P(x_A) dx_A = 1 - x_A^{\text{coex}(1)} \quad . \quad (5)$$

If there were no symmetry between A and B, $x_A^{\text{coex}(1)}$ and $x_A^{\text{coex}(2)}$ would be no longer related via Eq. (5). In this case the “successive umbrella sampling” would allow to locate both concentrations $x_A^{\text{coex}(1)}$ and $x_A^{\text{coex}(2)}$ by the “equal weight rule” [BC96, BH02].

Five independent runs were made for $N = 1600$, storing ten statistically independent states, whose concentration is as close to $x_A^{\text{coex}(2)}$ as possible (note that x_A is quantized in steps of $1/N$). These 50 configurations (at each T) were used as starting states for MD runs (in the microcanonical NVE ensemble where the energy is conserved [BC96]), using the “velocity Verlet algorithm” [BC96] as time integrator, with a time step $\delta t = 0.01$, in units of the standard LJ time unit [BC96] $t_0 = (m\sigma^2/48\epsilon)^{1/2}$. In order to work in the one-phase region, one can “heat up” the configurations gotten from MC at fixed x_B , and equilibrate the system by MD (the desired temperature is obtained by coupling the system to a stochastic heat bath [DHB03]).

It turns out that $N = 1600$ particles are enough to locate the coexistence curve rather precisely, the critical temperature is estimated with an accuracy better than 0.5%. If needed, much better accuracy could be achieved by a careful finite size scaling analysis [BC96, BH02]. In the following, the physical properties of the system along three paths will be described (Fig. 3): along the coexistence curve; at constant composition $x_B = 0.10375$, changing the temperature; and at the isotherm $T = 1.5$, crossing the one-phase region up to the coexistence curve.

4 Static properties

A static property of central interest in all simulations of fluids are radial distribution functions [BC96]. In a binary system three types of distribution functions have to be distinguished, $g_{AA}(r)$, $g_{AB}(r)$, and $g_{BB}(r)$. These are defined as

$$g_{\alpha\beta}(r) = \frac{N}{\rho N_A N_B} \left\langle \sum_{i=1}^{N_\alpha} \sum_{j=1}^{N_\beta} \frac{\delta(r - |\mathbf{r}_i(0) - \mathbf{r}_j(0)|)}{4\pi r^2} \right\rangle \quad . \quad (6)$$

As an example, Fig. 4 shows these partial radial distribution functions for a state at the coexistence curve at $T = 1.2$. Although the model is symmetric between A and B, $g_{AA} \neq g_{BB}$. This happens, because along the A-rich branch of the coexistence curve, the concentration of B particles is less than that of

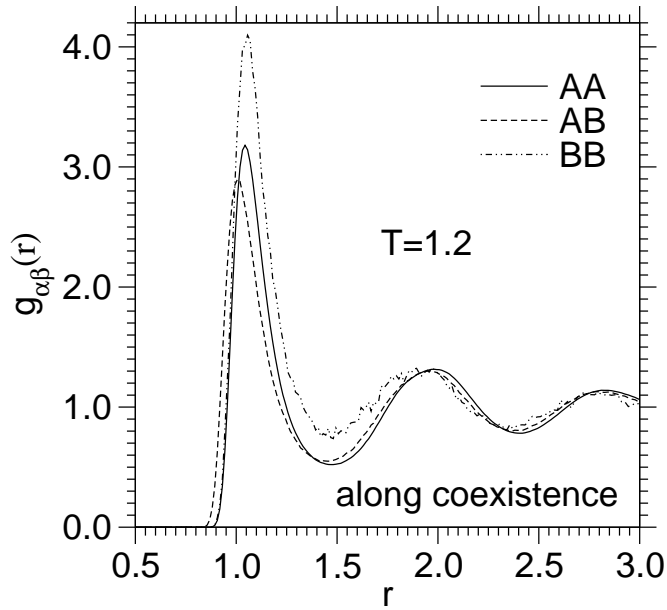


Fig. 4. Radial distribution function $g_{AA}(r)$ (solid line), $g_{AB}(r)$ (dashed line), and $g_{BB}(r)$ (dashed-dotted line) plotted vs. r , for a state at the coexistence curve at $T = 1.2$. From [DHB03].

A particles. When one increases the temperature, this difference gets smaller and ultimately must vanish at the critical point.

Of particular interest are also the static structure factors $S_{\alpha\beta}(q)$, since these quantities in principle are experimentally accessible in elastic scattering experiments (e.g. neutron scattering with momentum transfer $\hbar q$). Again one has to distinguish three partial structure factors, defined according to

$$S_{\alpha\beta}(q) = \frac{f_{\alpha\beta}}{N} \sum_{k=1}^{N_\alpha} \sum_{l=1}^{N_\beta} \langle \exp[i\mathbf{q} \cdot (\mathbf{r}_k - \mathbf{r}_l)] \rangle \quad (7)$$

with $f_{\alpha\beta} = 1$ for $\alpha = \beta$ and $f_{\alpha\beta} = 0.5$ for $\alpha \neq \beta$. From the partial structure factors one can form various combinations of physical interest, such as the number density structure factor $S_{nn}(q)$,

$$S_{nn}(q) = S_{AA}(q) + 2S_{AB}(q) + S_{BB}(q) \quad . \quad (8)$$

$S_{nn}(q)$ would show up in scattering of radiation that does not distinguish between the particles. Fig. 5 shows that $S_{nn}(q)$ appears to behave as any ordinary (almost incompressible) fluid {note that $S_{nn}(q \rightarrow 0)$ is related to the isothermal compressibility [BC96]}. There is no sign in this quantity that a critical point of unmixing is approached. However, there is another combination [Zim79],

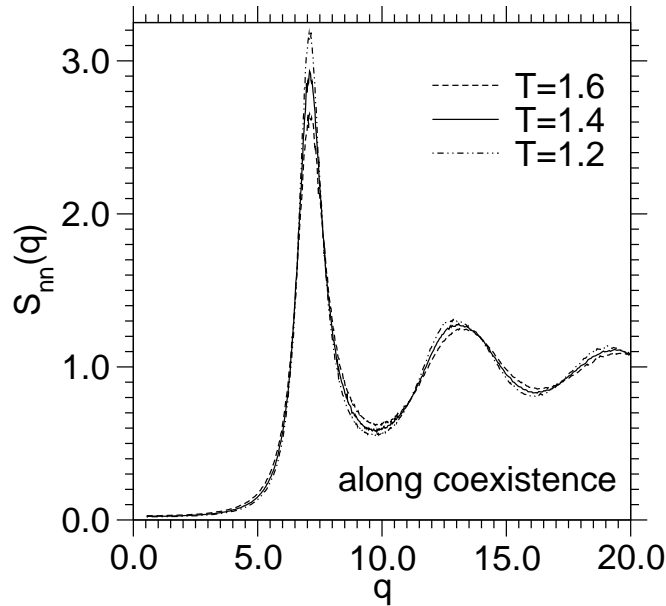


Fig. 5. Structure factor $S_{nn}(q)$ plotted vs. q , for the three indicated temperatures, choosing states along the coexistence curve. From [DHB03].

$$S_{cc}(q) = x_B^2 S_{AA}(q) + x_A^2 S_{BB}(q) - 2x_A x_B S_{AB}(q) , \quad (9)$$

which is basically the Fourier transform of the correlation function $g_{cc}(r)$ of concentration fluctuations $\{g_{cc}(r) = x_A^2 x_B^2 [g_{AA}(r) + g_{BB}(r) - 2g_{AB}(r)]\}$.

It is remarkable that $g_{cc}(r)$ exhibits a negative peak around $r \approx 0.9$ (Fig. 6). This indicates an anti-correlation in the concentration density fluctuations which stems from the fact that distances around $r = 0.9$ are avoided by nearest A–A and B–B neighbors but are typical for nearest A–B neighbors. While $g_{cc}(r)$ is almost zero at low temperatures and in addition very short-ranged (Fig. 6), it develops a stronger peak and a more long-ranged slow decay as one approaches criticality. One expects $g_{cc} \propto r^{-1} \exp(-r/\xi)$, ξ being the correlation length of concentration fluctuations. The maximum value of $S_{cc}(q)$ occurs for $q = 0$. This maximum could never be directly estimated from a microcanonical MD simulation, where the number of A particles as well as the number of B particles is fixed and thus $S_{cc}(q = 0) = 0$ (in this case the nonzero maximum rather would be defined via the limit $S_{cc}(q \rightarrow 0^+)$). However, the semigrandcanonical MC calculation allows to estimate this quantity via a simple fluctuation relation,

$$S(q = 0) = k_B T \chi = N \left\{ \int_{1/2}^1 x_A^2 P(x_A) dx_A - [x_A^{\text{coex}(1)}]^2 \right\} . \quad (10)$$

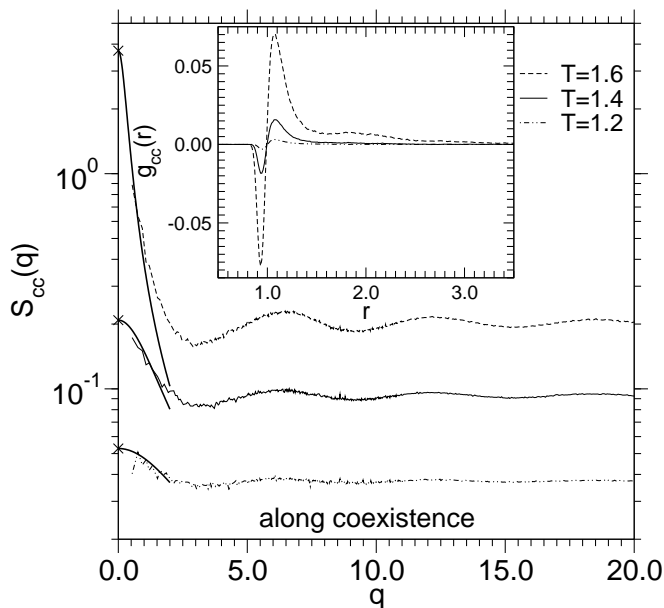


Fig. 6. Concentration fluctuation structure factor $S_{cc}(q)$ plotted vs. q , for three temperatures as indicated, choosing states along the coexistence curve. Note the logarithmic scale of the ordinate. Crosses at the ordinate represent the “susceptibility” $k_B T \chi$ (see text), while the bold solid lines are fits to the Ornstein–Zernike equation $S_{cc}(q) = k_B T \chi / [1 + q^2 \xi^2]$, which should hold at small q . Inset shows the correlation function $g_{cc}(r)$. From [DHB03].

The values of $k_B T \chi$ as obtained by Eq. (10) are shown in Fig. 6 as crosses at $q = 0$.

Interestingly, there is also a nonzero cross correlation between concentration and density fluctuations. This is measured via the function $g_{nc}(r) = x_A x_B [x_A g_{AA}(r) - x_B g_{BB}(r) + (x_B - x_A) g_{AB}(r)]$ or the corresponding structure factor $S_{nc}(q)$,

$$S_{nc}(q) = x_B S_{AA}(q) - x_A S_{BB}(q) + (x_B - x_A) S_{AB}(q) \quad . \quad (11)$$

If one would work exactly at $x_A = x_B = 1/2$ for $T > T_c$, symmetry would require that $S_{nc}(q) \equiv 0$. So it is plausible that along the coexistence curve this quantity is still rather small (Fig. 7).

The same structure factors have also been studied for the other paths included in the phase diagram, Fig. 3. As an example, Fig. 8 shows $S_{cc}(q)$ for an isotherm at $T = 1.5$. Further simulation data can be found in [DHB03].

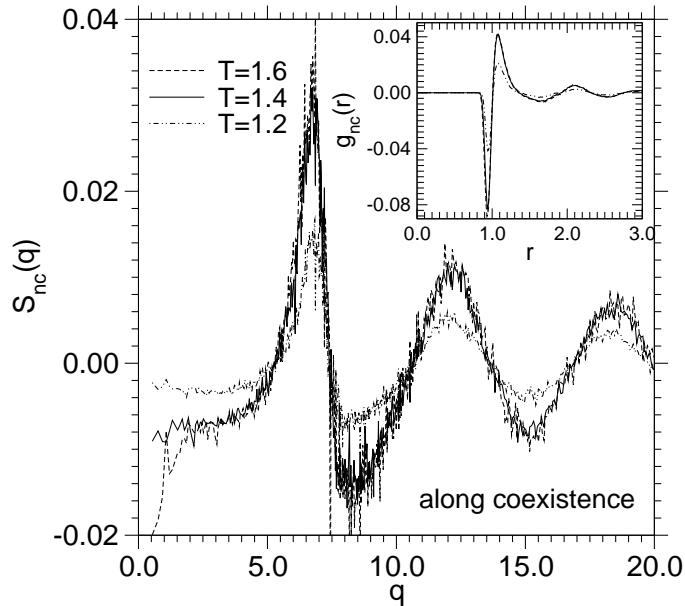


Fig. 7. Cross correlation structure factor $S_{nc}(q)$ plotted vs. q , for three temperatures as indicated, choosing states along the coexistence curve. The inset shows the correlation function $g_{nc}(r)$. From [DHB03].

5 Dynamic properties

A quantity that contains information on how the various kinds of particles move, and that is experimentally accessible e.g. via incoherent inelastic scattering of neutrons, is the incoherent intermediate scattering function $F_s^{(\alpha)}(q, t)$,

$$F_s^{(\alpha)}(q, t) = \frac{1}{N_\alpha} \sum_{i \in \alpha} \langle \exp\{-i\mathbf{q} \cdot [\mathbf{r}_i(0) - \mathbf{r}_i(t)]\} \rangle, \quad \alpha \in (A, B) \quad . \quad (12)$$

Fig. 9 shows this quantity for the A particles, including three states along the coexistence curve. The decay of this function with time t obviously becomes very slow when q becomes small. This observation simply describes the “hydrodynamic slowing down”: the relaxation times diverge as expected from diffusive behavior. A simple argument to see this assumes the displacements $\mathbf{r}_i(0) - \mathbf{r}_i(t)$ to be Gaussian distributed at long enough times, which yields $F_s^{(\alpha)}(q, t) = \exp[-q^2 g_\alpha(t)/6]$, where $g_\alpha(t)$ is the mean square displacement of species α ,

$$g_\alpha(t) = \langle [\mathbf{r}_{i,\alpha}(0) - \mathbf{r}_{i,\alpha}(t)]^2 \rangle \quad . \quad (13)$$

Using now the Einstein relation, $g_\alpha(t) = 6D_\alpha t$ for $t \rightarrow \infty$, one notes that $F_s^{(\alpha)}(q, t) \propto \exp[-t/\tau_\alpha(q)]$ with $\tau_\alpha(q) = (D_\alpha q^2)^{-1}$. Fig. 10 shows that this

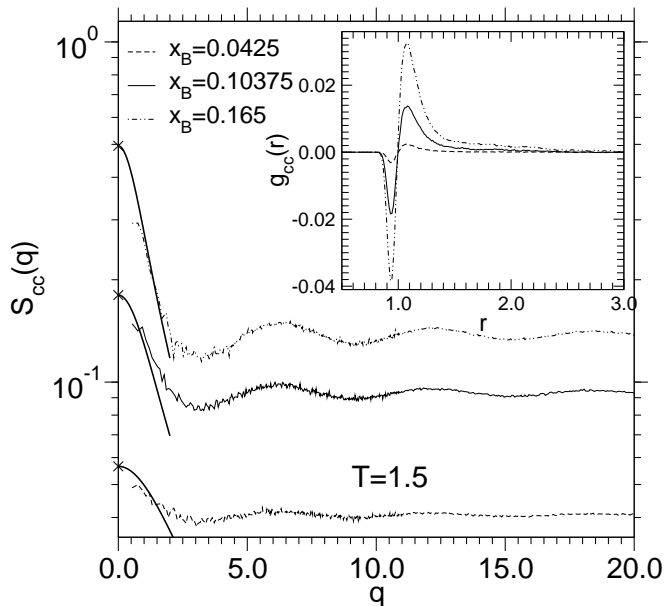


Fig. 8. Concentration fluctuation structure factor $S_{cc}(q)$ plotted vs. q , at $T = 1.5$ and three concentrations as shown. The inset shows $g_{cc}(r)$. For further explanations see Fig. 6. From [DHB03].

interpretation indeed is compatible with the MD results for $q \rightarrow 0$. This hydrodynamic slowing down is a general consequence of the fact that in the microcanonical MD simulation the concentrations $x_A = N_A/N$, $x_B = N_B/N$ are conserved quantities: Therefore, long-wavelength concentration fluctuations, if they were present in the system, would take a very long time to equilibrate. Clearly, this equilibration problem is avoided by the equilibration with Monte Carlo methods in the semigrandcanonical ensemble.

Fig. 11 presents data on the coherent intermediate scattering function $F_{\alpha\beta}(q, t) \equiv S_{\alpha\beta}(q, t)/S_{\alpha\beta}(q, 0)$ where

$$S_{\alpha\beta}(q, t) = \frac{f_{\alpha\beta}}{N} \sum_{i \in \alpha} \sum_{j \in \beta} \langle \exp\{-i\mathbf{q} \cdot [\mathbf{r}_i(t) - \mathbf{r}_j(0)]\} \rangle \quad (14)$$

with $f_{\alpha\beta} = 1$ for $\alpha = \beta$ and $f_{\alpha\beta} = 0.5$ for $\alpha \neq \beta$. From $F_{AA}(q, t)$ {Fig. 11} one can clearly recognize that several relaxation processes contribute, since the decay occurs in several steps. In contrast, in the concentration correlation function $F_{cc}(q, t)$ only a single step (representing the slowest decay) is found (Fig. 12). For the cases that were studied, the relaxation time describing this "slow" decay is not yet much slower than the decay times $\tau_A(q)$ and $\tau_B(q)$ of the self-correlation functions, Figs. 9 and 10. However, taking data close to the critical point one expects that the collective time scale seen in $F_{cc}(q, t)$

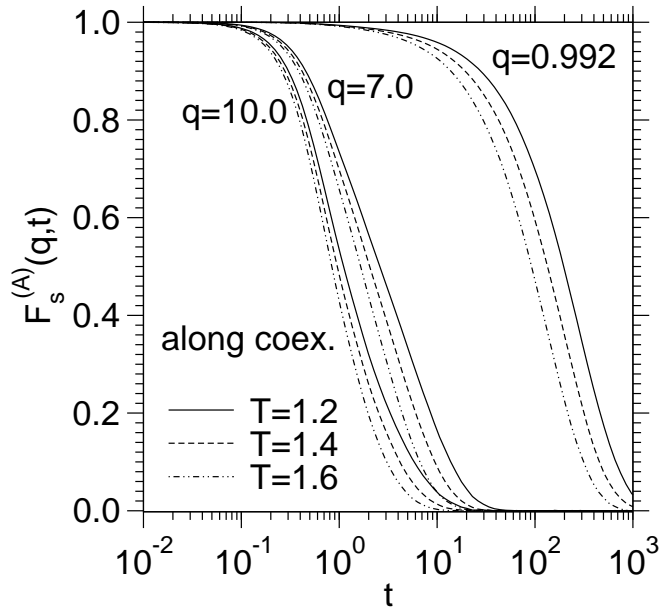


Fig. 9. Incoherent intermediate scattering function of A particles plotted vs. time (note the logarithmic scale of time) for three temperatures and concentrations, along the A-rich part of the coexistence curve, $T = 1.2$ (solid lines), $T = 1.4$ (dashed lines), and $T = 1.6$ (dashed-dotted lines). Each panel shows $F_s^{(A)}(q, t)$ for 3 values of q , namely $q = 0.992, 7, 10$ (from right to left). From [DHB03].

should become very much larger than the single-particle timescales $\tau_A(q)$ and $\tau_B(q)$, which are related to selfdiffusion, as noted above. One does not expect any significant slowing down of selfdiffusion when one approaches the critical point [KBK82]. In contrast, $F_{cc}(q, t)$ should pick up the decay described by the interdiffusion constant [KBR89]: in addition to the “hydrodynamic slowing down” shown by all relaxation times relating the diffusion because of the conservation laws for the concentration of particles [KM63], there is also “critical slowing down” [HH77], i.e. the interdiffusion constant vanishes as $T \rightarrow T_c$, and this slow decay one expects to see in $F_{cc}(q, t)$. However, for the choices of T presented this is not yet evident, since the onset of critical slowing down in this regime of temperature is to a large extent offset by a general slowing down of all transport phenomena as the temperature is lowered.

This ordinary slowing down (which often is described by simple Arrhenius laws for transport coefficients, e.g. $\ln(D_{\alpha\beta}) = -E_{\alpha\beta}/T + \text{const.}$, $E_{\alpha\beta}$ being an activation energy) can be studied conveniently when one follows a path at constant concentration in the one-phase region above the coexistence curve, such as the path at $x_B = 0.10375$ included in Fig. 3. The corresponding results are shown in Fig. 13, where the selfdiffusion coefficients D_A , D_B are shown

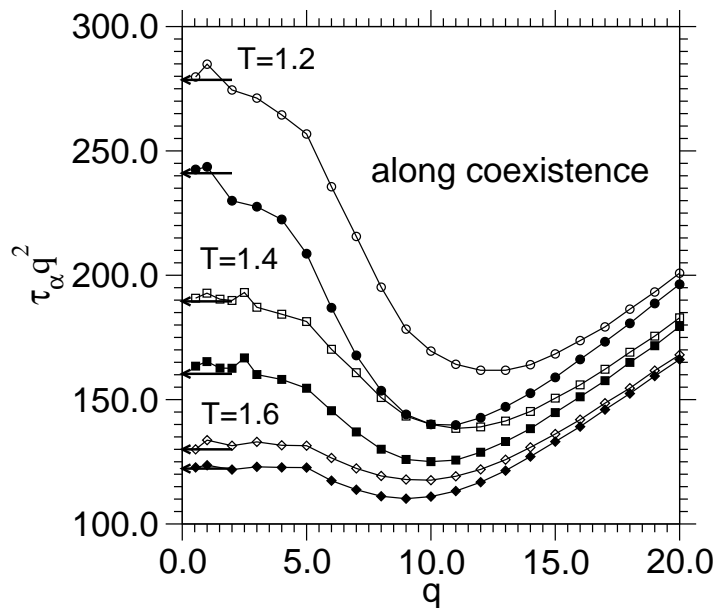


Fig. 10. Plot of the scaled relaxation time $\tau(q)q^2$ vs. q , for the A particles (open symbols), and the B particles (filled symbols), for three temperatures along the A-rich branch of the coexistence curve. The arrows indicate the values of the corresponding inverse selfdiffusion constants, as estimated from the Einstein relation. From [DHB03].

together with the inverse shear viscosity η^{-1} and the interdiffusion coefficient D_{int} , as extracted from Green-Kubo formulas [BY80]. These relations are

$$\eta = \frac{1}{Vk_B T} \int_0^\infty dt \langle \sigma_{xy}(0) \sigma_{xy}(t) \rangle \quad (15)$$

where $\sigma_{xy}(t)$ is an off-diagonal component of the pressure tensor defined by

$$\sigma_{xy}(t) = \sum_i \left(m_i v_{ix} v_{iy} + \frac{1}{2} \sum_{j \neq i} |x_i - x_j| F_y(|\mathbf{r}_i - \mathbf{r}_j|) \right), \quad (16)$$

\mathbf{v}_i being the velocity of the i 'th particle, and $\mathbf{F}(|\mathbf{r}_i - \mathbf{r}_j|)$ is the force acting on particle i due to the (pairwise) interaction with particle j . The sum \sum_i in Eq. (16) extends over both kinds of particles, unlike Eq. (14). A similar relation can also be formulated for the interdiffusion coefficient, namely

$$D_{\text{int}} = \frac{1}{NS_{\text{cc}}(0)} \int_0^\infty dt \langle j_x^{\text{int}}(0) j_x^{\text{int}}(t) \rangle, \quad (17)$$

with the interdiffusion current given by

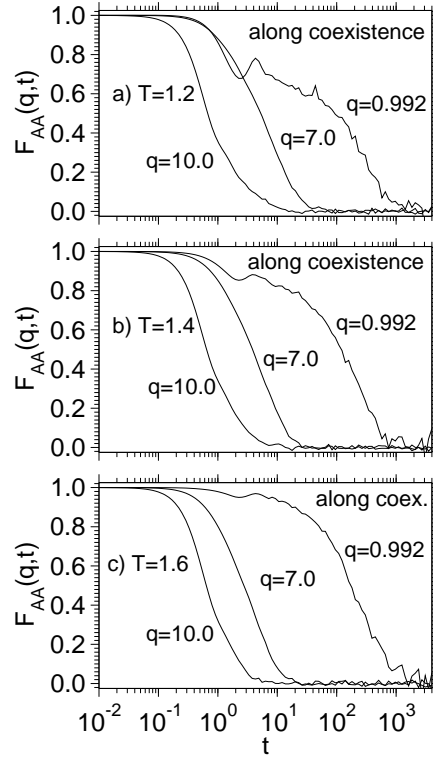


Fig. 11. Coherent intermediate scattering function $F_{AA}(q, t)$ of A particles plotted vs. time (note the logarithmic scale of time). Three temperatures are shown at states along the coexistence curve: $T = 1.2$ (a), $T = 1.4$ (b), and $T = 1.6$ (c). Three wavenumbers are included as indicated. From [DHB03].

$$\mathbf{j}_{\text{int}}(t) = x_B \sum_{i=1}^{N_A} \mathbf{v}_i(t) - x_A \sum_{i=1}^{N_B} \mathbf{v}_i(t) \quad . \quad (18)$$

From Fig. 13 it is evident that all transport coefficients D_A , D_B , D_{int} and η^{-1} decrease as one lowers the temperature, but simple Arrhenius relations do not hold. In addition, we note that for the minority component the selfdiffusion constant always is a bit faster than for the majority component. The interdiffusion constant has a value which is hardly different from the selfdiffusion constants at high temperatures, but becomes appreciably smaller than the latter when one approaches the coexistence curve. Recall, as noted above, one expects $D_{\text{int}} \rightarrow 0$ if the path $x_B = x_B^{\text{crit}} = 1/2$ would be chosen so that one approaches the critical point, while for the strongly off-critical case considered in Fig. 13 $D_{\text{int}} \neq 0$ at the coexistence curve, of course.

The results for the viscosity allow a check of the Stokes–Einstein formula for the selfdiffusion constants

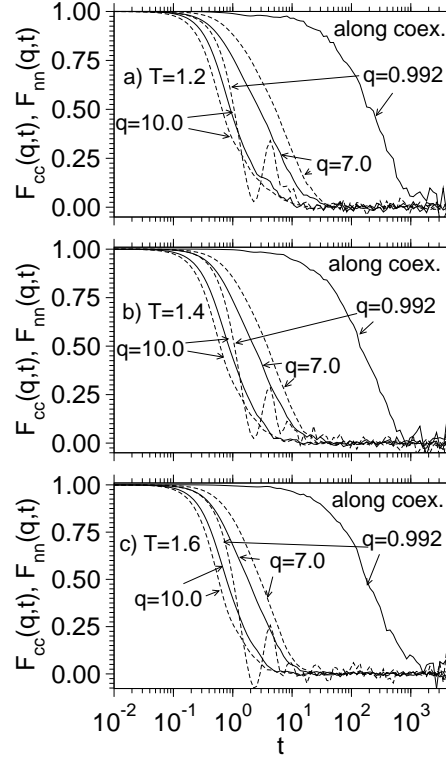


Fig. 12. Concentration–concentration correlation functions $F_{cc}(q, t) = S_{cc}(q, t)/S_{cc}(q, 0)$ plotted vs. time. Here $S_{cc}(q, t)$ is the dynamic counterpart of the function $S_{cc}(q)$ defined in Eq. (9). Three states along the coexistence are shown with $T = 1.2$ (a), $T = 1.4$ (b), and $T = 1.6$ (c). Curves for the same wavenumbers q as shown in Fig. 11 are included. From [DHB03].

$$D_\alpha = \frac{k_B T}{2\pi\eta d_\alpha} \quad , \quad (19)$$

d_α being the (effective) diameter of the corresponding particle species $\alpha \in \{A, B\}$. If Eq. (19) were strictly correct, one would expect $d_A \approx \sigma_A = 1$ and $d_B \approx \sigma_B = 1$. It turns out that this would be a reasonable approximation for the A particles, while for the B particles the result rather is $d_A \approx 0.8$ [DHB03]. Note that Eq. (19) is a widely used approximation, but it really lacks a good theoretical foundation: so this deviation of the simulation data from Eq. (19) is not really surprising.

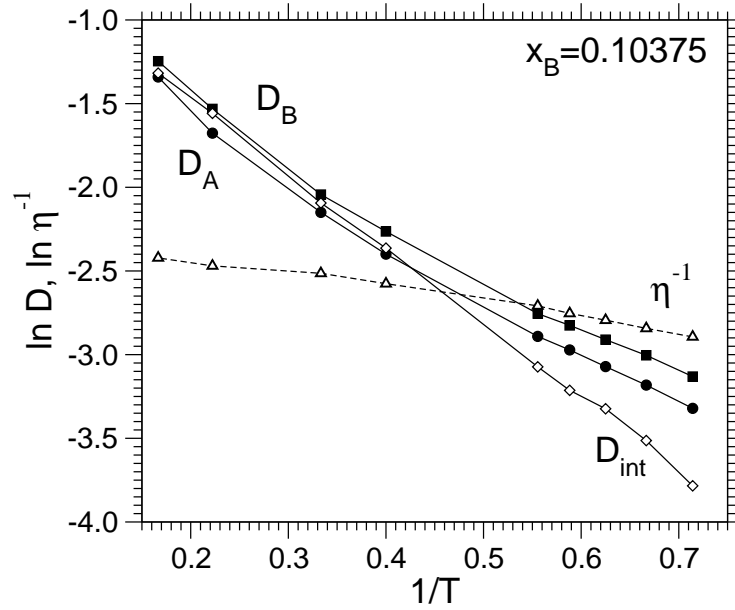


Fig. 13. Logarithm of the selfdiffusion constants D_A , D_B , the interdiffusion constant D_{int} , and the inverse viscosity η^{-1} plotted vs. inverse temperature for the mixture at constant concentration $x_B = 0.10375$. From [DHB03].

6 Discussion and outlook

Even for the simple model system of a symmetrical Lennard–Jones mixture there remains a lot to be done: the critical region needs to be explored for much larger particle numbers N , in conjunction with a finite size scaling analysis, to probe the theoretical predicted critical singularities [HH77] of the various transport coefficients. Such a study has never been carried out before.

Then it would be very interesting to simulate “quenching experiments” where one e.g. suddenly changes the temperature (at fixed x_A , x_B) from a state above the coexistence curve to a state below it, bringing the system into the two–phase region. Then the initially homogeneous state is unstable and will decay by either nucleation and growth (if the state point is close enough to the coexistence curve so that the homogeneous state is metastable) or by “spinodal decomposition” [Kos01]. Simulations of these processes are available for various models of solid mixtures (e.g. kinetic Ising models of rigid solid binary alloys) and in the framework of numerical work with suitable differential equations (e.g. the nonlinear Cahn–Hilliard equation [Kos01]), but atomistic simulations of these processes for liquid binary mixtures are not yet available. Such simulations are rather demanding, however, since the inhomogeneous two–phase structures that form are characterized by length scales much larger than the atomic diameters. Other interesting projects for this

model (some of them are already in progress!) consider confinement effects in slit capillaries of nanoscopic size, nonlinear flow problems, etc.

However, the real challenge is to carry the strategy described in the present paper over to chemically realistic models of real materials. Note that there is nontrivial structure in the pair correlation functions (Figs. 6 and 7) on scales much less than the Lennard–Jones parameters (describing such effects for real materials will require very accurate interatomic potentials as an input, which often are not yet available), in addition to the structure on the scale of the correlation length ξ (which grows to large values near the critical point). Real binary systems never have strictly symmetric miscibility gaps, and then phase coexistence occurs (in the semigrandcanonical ensemble) along a nontrivial curve $\Delta\mu_{\text{coex}}(T)$ in the $(\Delta\mu, T)$ plane. Mapping out the coexistence curve is a much harder task (though this can be done with the successive umbrella sampling technique [VM03]). One should also note that for asymmetric mixtures the A→B identity switch step may suffer from very low acceptance rates and suitable biasing schemes may need to be developed.

If all these problems could be solved, the present approach can yield very important input information for problems dealing with fluids on mesoscopic scales (where techniques such as Lattice–Boltzmann can be applied) or even macroscopic scales (where methods of computational fluid dynamics can be applied). The present approach therefore is potentially useful for applications in many fields (e.g. flow of oil plus water through porous rocks, flow of multiphase mixtures of polymers in the processing of plastic materials, flow of molten silicates in geophysical problems, etc.), but there remains still a long way to go until this will become a standard ingredient of multiscale simulation approaches.

Acknowledgments: One of us (S. K. D.) was supported by the Deutsche Forschungsgemeinschaft (DFG) und grant N° Bi314-18 (SPP1120), another (J. H.) by DFG grant HO2231/2-1, another (M. M.) by a Heisenberg stipend, R. V. by SFB TR6 (A5). P. V. was partially supported by the Bundesministerium für Bildung und Forschung (BMBF) under grant N° 03N6015.

References

- [BC96] Binder, K., Ciccotti, G. (eds.): *Monte Carlo and Molecular dynamics of Condensed Matter Systems*, Italian Physical Society, Bologna (1996)
- [BH02] Binder, K., Heermann, D. W.: *Monte Carlo Simulations in Statistical Physics. An Introduction, 4'th edition*, Springer, Berlin (2002)
- [Bin82] Binder, K.: *Monte Carlo calculation of the surface tension for two- and three-dimensional lattice-gas models*, Phys. Rev. A **25**, 1699–1709 (1982)
- [Bin94] Binder, K.: *Phase transitions in polymer blends and block copolymer melts: some recent developments*, Adv. Polymer Sci. **112**, 181–299 (1994)
- [Bin95] Binder, K.: *Monte Carlo and Molecular Dynamics Simulations in Polymer Science*, Oxford University Press, New York (1995)

- [BK99] Bach, H., Krause, D. (eds.): *Characterization of Structure and Properties of Glass*, Springer, Berlin (1999)
- [BY80] Boon, J. P., Yip, S.: *Molecular Hydrodynamics*, McGraw Hill, New York (1980)
- [DHB03] Das, S. K., Horbach J., Binder, K.: *Transport phenomena and microscopic structure in partially miscible binary fluids: A simulations study of the symmetrical Lennard–Jones mixture*, J. Chem. Phys. **119**, 1547–1558 (2003)
- [HH77] Hohenberg, P. C., Halperin, B. I.: *Theory of dynamic critical phenomena*, Rev. Mod. Phys. **49**, 435–479 (1977)
- [Jae86] Jäckle, J.: *Models of the glass transition*, Rep. Progr. Phys. **49**, 171–231 (1986)
- [KBK82] Kutner, R., Binder, K., Kehr, K. W.: *Diffusion in concentrated lattice gases. II. Particles with attractive nearest-neighbor interaction on three-dimensional lattices*, Phys. Rev. B **26**, 2967–2980 (1982)
- [KBR89] Kehr, K. W., Binder, K., Reulein, S. M.: *Mobility, interdiffusion, and tracer diffusion in lattice-gas models of two-component alloys*, Phys. Rev. B, **39**, 4891–4910 (1989)
- [KM63] Martin, P., Kadanoff, L. P.: *Hydrodynamic equations and correlation functions*, Ann. Phys. (NY) **24**, 419–469 (1963)
- [Kos01] Kosterz, G. (ed.): *Phase Transformations in Materials*, Wiley-VCH, Berlin (2001)
- [VM03] Virnau, P., Müller, M.: *Successive umbrella sampling*, preprint (2003)
- [Zim79] Ziman, J. M.: *Models of Disorder*, Cambridge University Press, Cambridge (1979)